applied sciences

MDPI

Article

Silicone Elastomeric-Based Materials of Soft Pneumatic Actuator for Lower-Limb Rehabilitation: Finite Element Modelling and Prototype Experimental Validation

Hanisah Bakeri [1,2], Khairunnisa Hasikin [1,3,*], Nasrul Anuar Abd Razak [1], Rizal Mohd Razman [4], Abd Alghani Khamis [5], Muhammad 'Ammar Annuha [1], Abbad Tajuddin [2] and Darween Reza [6]

1 Department of Biomedical Engineering, Faculty of Engineering, Universiti Malaya, Kuala Lumpur 50603, Malaysia
2 Medical Revolution Sdn. Bhd, 10 Boulevard, Petaling Jaya 47400, Malaysia
3 Center of Intelligent Systems for Emerging Technology (CISET), Faculty of Engineering, Universiti Malaya, Kuala Lumpur 50603, Malaysia
4 Faculty of Sports and Exercise Science, Universiti Malaya, Kuala Lumpur 50603, Malaysia
5 Department of Mechanical Engineering, Faculty of Engineering, Universiti Malaya, Kuala Lumpur 50603, Malaysia
6 My Conceptual Robotics Sdn. Bhd (MyCRO), Kompleks Diamond, Bandar Baru Bangi 43650, Malaysia
* Correspondence: khairunnisa@um.edu.my

Abstract: This study describes the basic design, material selection, fabrication, and evaluation of soft pneumatic actuators (SPA) for lower-limb rehabilitation compression therapy. SPAs can be a promising technology in proactive pressure delivery, with a wide range of dosages for treating venous-related diseases. However, the most effective design and material selection of SPAs for dynamic pressure delivery have not been fully explored. Therefore, a SPA chamber with two elastomeric layers was developed for this study, with single-side inflation. The 3D deformation profiles of the SPA chamber using three different elastomeric rubbers were analyzed using the finite element method (FEM). The best SPA-compliant behavior was displayed by food-grade silicone A10 Shore with a maximum deformation value of 25.34 mm. Next, the SPA chamber was fabricated using A10 Shore silicone and experimentally validated. During the simulation in FEM, the air pressure was applied on the inner wall of the chamber (i.e., the affected area). This is to ensure the applied pressure was evenly distributed in the inner wall while the outer wall of the chamber remained undeformed for all compression levels. During the inflation process, pressure will be applied to the SPA chamber, causing exerted pressure on the skin which is then measured for comparison. The simulation and experimental results show an excellent agreement of pressure transmission on the skin for the pressure range of 0–120 mmHg, as depicted in the Bland–Altman plots. The findings exhibited promising results in the development of the SPA chamber using low-cost and biocompatible food-grade silicone.

Keywords: compression therapy; finite element modelling (FEM); hyperelastic material; soft pneumatic actuator (SPA); lower limb; silicone elastomer; venous disease

check for updates

Citation: Bakeri, H.; Hasikin, K.; Abd Razak, N.A.; Mohd Razman, R.; Khamis, A.A.; Annuha, M.'A.; Tajuddin, A.; Reza, D. Silicone Elastomeric-Based Materials of Soft Pneumatic Actuator for Lower-Limb Rehabilitation: Finite Element Modelling and Prototype Experimental Validation. *Appl. Sci.* **2023**, *13*, 2977. https://doi.org/10.3390/app13052977

Academic Editor: Ana Martins Amaro

Received: 30 December 2022
Revised: 21 February 2023
Accepted: 22 February 2023
Published: 25 February 2023

Copyright: © 2023 by the authors. Licensee MDPI, Basel, Switzerland. This article is an open access article distributed under the terms and conditions of the Creative Commons Attribution (CC BY) license (https://creativecommons.org/licenses/by/4.0/).

1. Introduction

Extremity trauma is one of the most common injuries perceived in emergency medical practice. These injuries are examined using four functional components (nerves, vasculature, bones, and soft tissues), whereby each component must be assessed individually as well as collectively. Injuries to the lower extremity are severe in all age groups, but individuals who engage in physical activity and sports are at an especially higher risk for severe trauma. An estimated 4.5 million sports- and physical-activity-related injuries have been reported, with a large percentage of these injuries being lower extremity injuries [1]. The highest cited injuries among all lower-limb-related injuries in runners are

patellofemoral pain (PFP), iliotibial band syndrome (ITBS), medial tibial stress syndrome (MTSS), Achilles tendinopathy (AT), plantar fasciitis, stress fractures, and muscle strains. Some of these injuries have a high recurrence rate, leading to a reduction or cessation of training in approximately 30% to 90% of cases [2].

Athletes suffering from lower-limb injuries, particularly muscular injuries, will experience time loss during both training and competition [3]. These muscle injuries account for the absence of up to 37% of players from training and matches [4]. The severity of muscle injury, particularly skeletal muscle disruption, can lead to chronic disease in several organ systems, including cardiovascular disease (CVD), neurological, endocrine, renal, gastrointestinal (GIT), metabolic diseases, and cancers [5]. The presence of edema caused by muscle injuries could lead to the compression of popliteal or gastrocnemius veins, resulting in deep vein thrombosis (DVT), while a faulty valve can cause venous blood pumped toward the heart to reflux, resulting in chronic venous insufficiency (CVI) [6].

In the general population, the average incidence rate of DVT is between 100 and 200 per 100,000 person-years [7]. With the increasing incidence of venous disorders, compression therapy is frequently deployed for the prevention and treatment of vasculopathy such as varicose veins, deep vein thrombosis, lymphatic edema, wound management, and pain reduction [8]. Compression therapy usually encompasses the use of multi-layered bandages, hosiery, compression garments, intermittent pneumatic compression, and complicated compression devices [9]. However, for individuals with limited body movements, applying compression would be tedious and might cause skin irritation which leads to skin damage. Thus, pneumatic compression therapy has recently been promoted as an alternative for treating patients who do not respond to conservative approaches. In a recent innovation by Luca Rosalia et al. [10], a soft robotic device for lower-limb compression was used in the treatment of lymphedema. This device expanded upon the technique pioneered by Low et al. [11], in which the actuation strength and motion could be customized based on user input.

Pneumatic compression devices often employ single or multiple pneumatic chambers or bladders to generate variable compression cycles by manipulating the air during the inflation–deflation modes. Soft actuators, notably air bladders, have been used in various applications, including space deployments and medical devices. This includes several soft pneumatic actuators (SPAs) made of linear or non-linear soft materials that provide various predetermined motions or forces.

Several researchers have attempted to use SPAs for the compression treatment of human limbs and joints, as shown in Table 1. The identification and selection of articles are restricted to research articles published between 2016 to 2022 to ensure that the content of the article and resources are comprehensive and up to date. The articles are based on three main areas of study, which are rehabilitation, soft actuators, and compression therapy. The strengths and weaknesses of soft actuators were presented based on these criteria.

Chua et al. [11] designed a soft robotic therapeutic glove for rheumatoid arthritis for the lateral compression and massage of the fingers and joints. Thalman et al. [12] introduced a soft robotic ankle foot orthosis (SRA-FO) exosuit based on a fabric-based pneumatic actuator that provided inversion and eversion ankle support as a form of gait rehabilitation, while Mengjia Zhu et al. [13] introduce fluidic fabric muscle sheets for wearable and soft robotics. Xiao et al. [14] designed a soft pneumatic interface between a crutch and the user's forearm using a fiber-reinforced elastomeric enclosure to decrease wrist and palmer loads. However, regardless of the SPA's usage in rehabilitation, creating it with biocompatible components that are both safe for humans and the environment remained elusive.

The simulation technique is important for designing, developing, and optimizing the soft robots' performance. Finite element modeling (FEM) is one of the approaches for modeling and simulating soft robotic components. The available compression models do not provide a timely quantification of the SPA unit, such as the interface pressure and treatment cycle. Thus, an irregular or unpredictable pressure dosage is delivered to

the body by the SPA unit [15]. The use of unpredictable or uneven pressure dosages in treatment may obstruct blood flow, resulting in cerebral, cardiac, and vascular illness [16]. The SPA pressure performance can be numerically analyzed using FEM to guide SPA material design selection and pressure dosage selection in therapy. Current studies aim to produce soft-bodied programmable motion inspired by biology aspects to combine natural compliance with controllable actuation [17–19]. Silicone rubber elastomers including the Smooth-On Ecoflex series (Smooth-On, Inc., Macungie, PA, USA), parts of the Dragon Skin series (Smooth-On, Inc., Macungie, PA, USA), and Sylgard 184 (Dow Corning Corporation, Midland, MI, USA) were predominantly used in the fabrication of soft actuators [20]. The lack of SPAs with a high strain density to transfer effective pressure while remaining nonhazardous is one of the challenges in this research area [21]. The simulations can be used for the instant and effective iteration between several designs and materials to enhance their functionality [22]. This affects the effectiveness of the treatment, user comfort, and frequency of application.

This research aims to address the issue by using FEM to anticipate the influence of the material selection of three silicone elastomeric rubbers composed of commercial and food-grade silicone, as well as conducting experimental testing to validate the SPA lower-limb system against simulation results. The SPA chamber's efficiency at transmitting pressure to a mannequin leg was also tested. The performance of silicone elastomeric rubbers was analyzed on the deformation structure of the chambers and force output with a correlation to the applied pressure and time.

Table 1. Summary of SPA for compression treatment of human lower-limb parts.

Author [Ref.]	Site of Application	Material	Functionalities	Advantages	Challenges
Chua et al. [11]	Fingers and Joints	Thermoplastic polyurethane (TPU)	Lateral compression for rheumatoid arthritis	Varying stiffness	Control-ability
Thalman et al. [12]	Ankle foot	200D TPU coated nylon	Provide inversion and eversion ankle support	Varying stiffness	Control-ability
Mengjia Zhu et al. [13]	Limbs	Fabric sheet	Wearable and soft robotics	Lightweight and low-cost	Untethered operation control-ability
Xiao et al. [14]	Wrist and palmer	Elastomers and fiber	To decrease wrist and palmer loads	Lightweight, effective	/
Fang et al. [23]	Knee	TPU fabric	Knee rehabilitation and movement	Lightweight, easy-to-control	On-board power source
Li et al. [24]	Hand	Soft latex	Passive hand rehabilitation for stroke patients	Low-cost, lightweight, easy-to-wear	No individual control of the finger

2. Materials and Methods

2.1. 3D-Modelling Construction

The conceptual model of the soft pneumatic actuator (SPA) was developed using the soft robotic toolkit as mentioned by [25]. The actuators were made up of two silicone parts: the main body and the bottom layer. The main body was composed of several chambers driven by a pressure source and inflated upon actuation. The actuators were designed to have one extendable side (top layer), while the other side was restrained or nonexpendable (bottom layer) as shown in Figure 1. The non-extendable layer of mesh fabric was embedded into the bottom part of the silicone layer to minimize the deformation of the bottom layer. To reduce the impact of additional pressure caused by the fabric's

stretch, a fabric with comparatively lower extension capability to the silicon layer was chosen. Polyester plain English net mesh fabric with a thickness of 0.008 was used. The fabric's thickness was sufficient to restrict the deformation of the outer layer. This fabric has an insignificant effect on the soft actuator's deformation due to its placement at the bottom layer of the SPA. This study focused on the deformation of the upper layer (chamber).

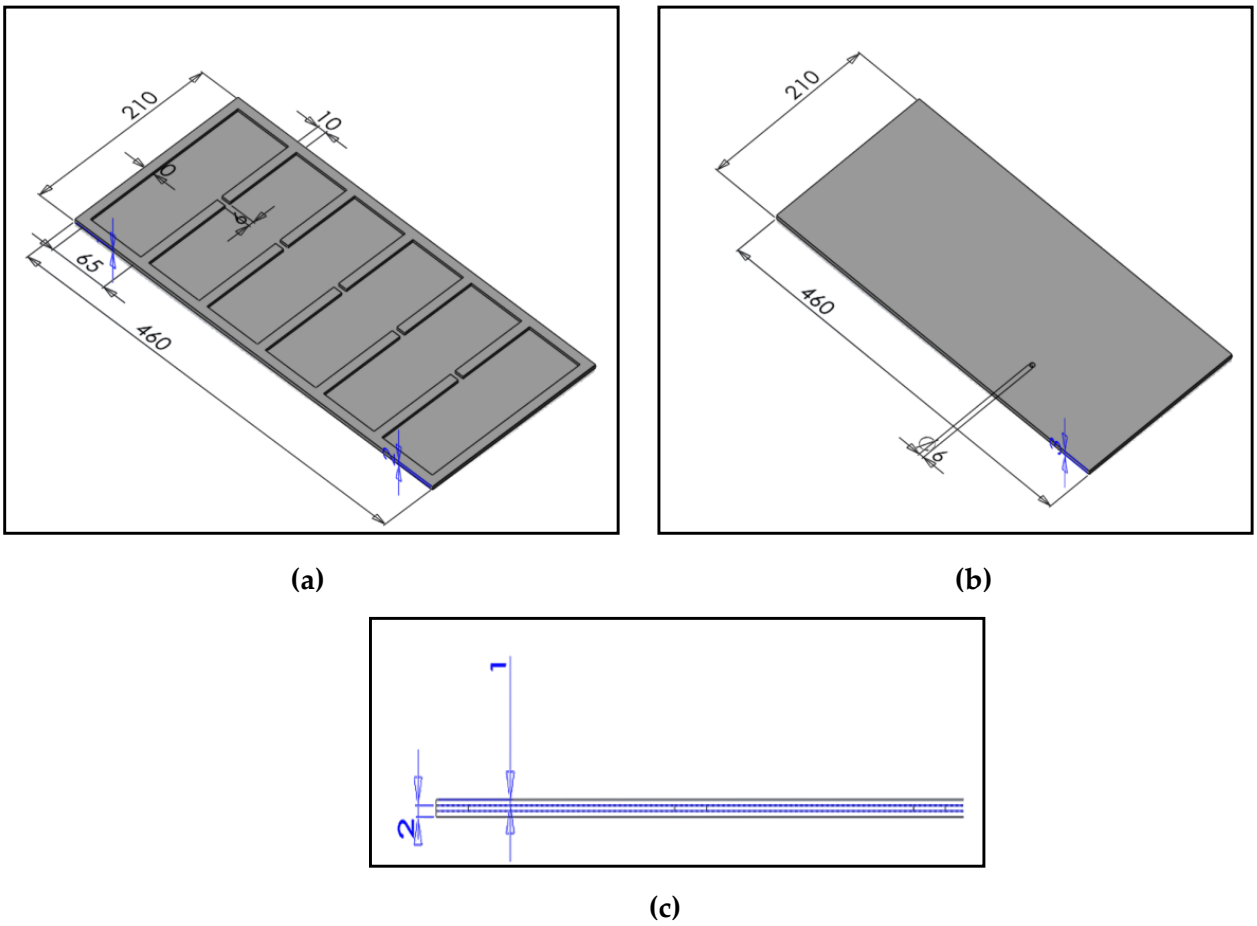


Figure 1. Dimension of 3D model construction of the proposed Model A SPA in mm: (**a**) top layer (**b**) nonexpendable bottom layer; and (**c**) side view.

Two SPA models, namely, Model A and Model B, were presented to examine the amount of pressure and the time required to inflate each chamber. Model A was designed with six chambers with one air inlet, whereas Model B was designed with six chambers with six separate inlets, in which both chambers were separated by a 10 mm gap with a side wall thickness of 1 mm. The chamber's shape and size were adaptive to the anatomy of the lower limb, with the 6 chambers compressing along part of the posterior and anterior of the lower leg to minimize dead volume. Each chamber was 65 mm in width and 190 mm in height. A 6 mm-diameter air inlet was fitted on the cuff shell to allow air supply from a pressure source to fill the chamber. Each chamber was connected by a channel for fluid flow as shown in Figure 2. The nonexpendable layer for each actuator has a thickness of 3 mm. The bottom layer was flexible to reduce the overall rigidity of the actuators. When the pressure was applied, the top layer of the chambers fully inflated, while the bottom layer had minimum to no inflation.

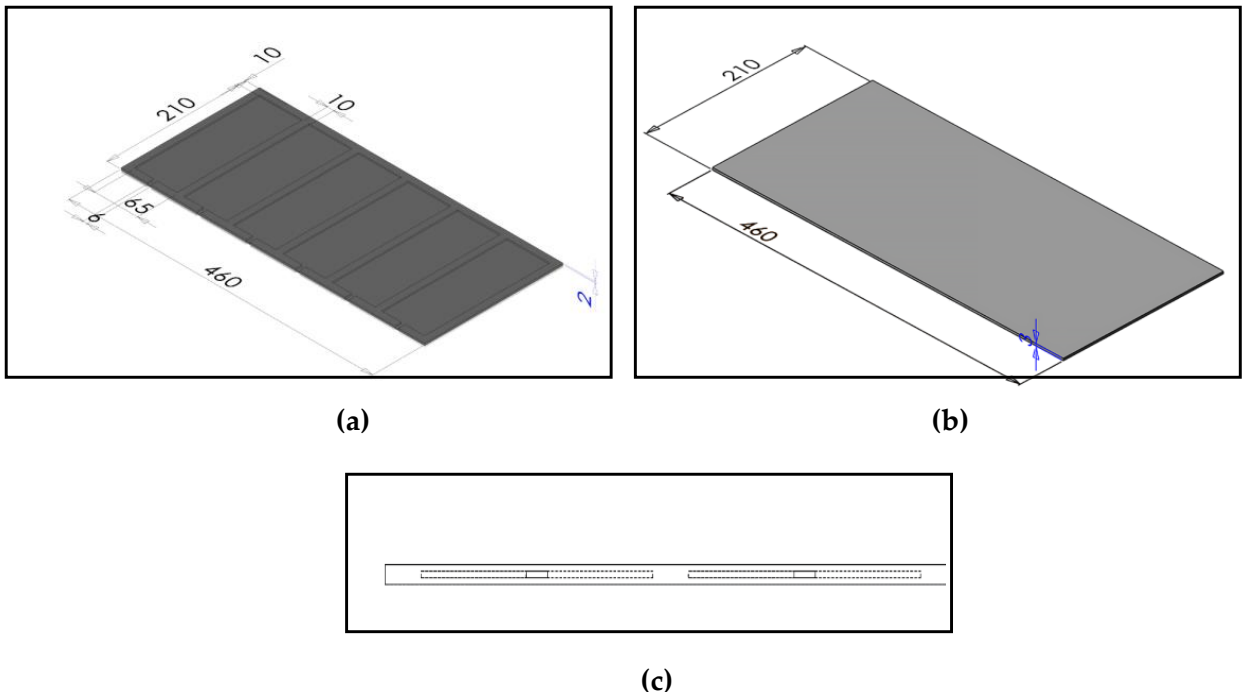


Figure 2. Dimension of 3D model construction of the proposed Model B in mm: (**a**) top layer (**b**) nonexpendable bottom layer; and (**c**) side view.

2.2. Material Properties and Characteristics

The crucial part of developing biocompatible and non-hazardous SPAs was the selection of suitable materials. Silicone elastomeric rubber is the most common material used in the 3D molding process to manufacture soft actuators [25]. In this study, we studied the properties of three different silicone-based materials as exhibited in Table 2.

The elastomeric materials model was used to describe the behavior of the selected silicone, with the characteristic of absorbing large deformation without permanent distortion. The silicone elastomeric rubber could withstand huge strains of 500% [26]. Silicone rubber has an elastic stress–strain curve with non-linear relation, and is isotropic, incompressible, and generally independent of strain rate. The most common non-linear constitutive model with incompressibility constraints such as Neo-Hookean, Ogden, Mooney–Rivlin, and Yeoh models have been considered for hyperelastic material [27]. These models can be represented by one or more material parameters that can be obtained from the stress–strain curve in experiments. Mooney–Rivlin model is mainly utilized in the study of rubber's small deformation range, whereas the Yeoh model is prioritized in the study of rubber's wide deformation range and is recommended for significant deformation [28].

The Yeoh model has the advantages of simplicity and excellent precision, and the material characteristics can be obtained through uniaxial compression experiments. The strain energy density function for Yeoh's 3rd model is given by:

$$W = C_1(I_1 - 3) + C_2(I_2 - 3)^2 + C_3(I_3 - 3)^3 \quad (1)$$

where C_1, C_2, and C_3 are model parameters, while I_1, I_2, and I_3 are strain invariants of Cauchy–Green deformation tensors, respectively. In this study, A15 Shore, A10 Shore, and Sylgard 184 were studied as the material of the proposed SPA system. The constitutive model parameters for three silicone elastomers and their properties are tabulated in Table 2. The Sylgard 184 model parameter was retrieved from Laura et al. [29] where the researchers use uniaxial tensile tests to identify the parameters of Yeoh models. In the ANSYS software (ANSYS 2019 R3), the A15 Shore is an elastomer. The model parameter values for A15 Shore

were retrieved from the ANSYS database [30] for the elastomer sample. The A10 Shore has the same properties as Dragon Skin 10 medium. The model parameters for A10 Shore were retrieved from Michele Di Lecce et al. [31], in which the researchers use Evolutionary Inverse Material Identification (EIMI) to identify the parameters of Yeoh models.

The three materials are flexible, extensible, and inexpensive. These silicones are highly resilient to deterioration and damage from extreme temperatures, non-toxic, and degradable [17]. However, for the optimal inflation and deflation of the proposed SPA, lower tensile strength was preferred to prevent persistent discomfort during compression.

Table 2. Material properties and constitutive model parameters of silicone elastomer.

	Sylgard 184	**A15 Shore**	**A10 Shore**
Manufacturer	Dow Corning	Clay art	Clay art
Color	Colourless	Translucent	Grey
Shore hardness	A50	A15	A10
Tensile strength	980 psi	537 psi	475 psi
Density	1.04 g/cm^3	1.35 g/cm^3	1.35 g/cm^3
Elongation at break	150%	771%	1000%
Durometer shore	50	15	10
Young's modulus	1.32–2.97 MPa	0.74 MPa	0.25 MPa
Model parameter	$C_1 = 0.42480$ MPa $C_2 = -0.15880$ MPa $C_3 = 0.24350$ MPa [29]	$C_1 = 0.69760$ MPa $C_2 = -0.24484$ MPa $C_3 = 0.12629$ MPa [30]	$C_1 = 0.00204$ MPa $C_2 = -0.17070$ MPa $C_3 = 2.05000$ MPa [31]

2.3. 3D Simulation of the Proposed Soft Pneumatic Actuator (SPA) System

To ensure the optimal deformation of the proposed SPA, the pressure distribution of the proposed 3D model and the proposed elastomeric materials (A15 Shore, A10 Shore, and Sylgard 184) was analyzed using the finite element method (FEM). The 3D model of the SPA was designed in Solidworks (Dassault Systèmes SOLIDWORKS Corp., Waltham, MA, USA) and then imported to ANSYS 2019 R3 for FEM analysis. It was assumed that the proposed compression system with a chamber should be able to provide homogeneous pressure regardless of the location of the cuff. For ensuring a balanced pressure, the air pressure was observed on the inner wall of the chamber. The SPA system for the analysis is shown in Figure 3 with fixed supports surrounding all edges highlighted in blue to imitate real-life behavior. Gravity was also considered for the solid domain, and it acted in the negative y direction.

Since this study employed elastomeric material, a physics nonlinear mechanics mesh with linear element order was adopted. The mesh method used for the SPA system was a hex-dominated element shape. Curvature and proximity capturing were activated. The experimental element size was set at 1 mm for all simulations which resulted in a total number of 300,196 elements. The minimum element quality based on skewness was 0.90.

In this study, a controlled condition of 23 s of inflates, 7 s of hold, and 7 s of deflate (23–7–7 s) in one cycle cumulating in 37 s was simulated. This method is a recommended treatment cycle by a commercially available intermittent pneumatic compression (IPC) device for daily home care of the lower limb [32]. The pressure was applied using the ramp function, with the gradual increment of the pressure from 0 to 120 mmHg from t = 0s to t = 23 s. Furthermore, in each simulation, the pressure was applied progressively throughout 44 sub-steps. This was a crucial variable because it prevents the load from being delivered entirely at once, which often leads to convergence problems, particularly when working with soft materials that have a low Young's modulus [33].

The three silicone elastomers' deforming structures affect the time and force with which they were applied to the skin. Additionally, they are highly dependent on the pressure, velocity, and material properties of silicone. The relationship between the input

pressure, the deformation, and the applicability of the developed 3D model was measured, based on the chamber's deformation profile.

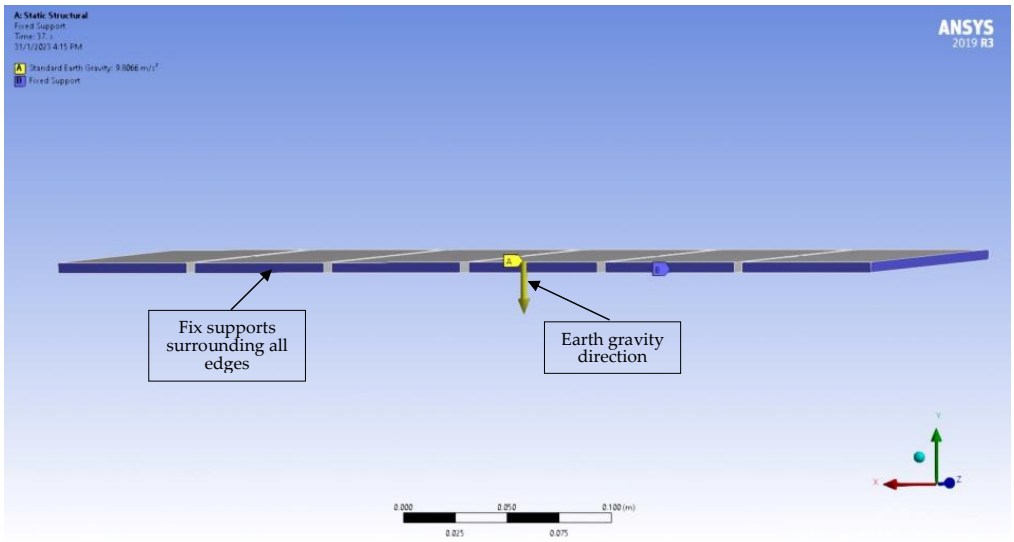


Figure 3. FEM simulation setting for SPA chamber. Fixed support surrounding the object and earth gravity applied in the negative y direction.

2.4. Experimental Analysis of SPA for Lower Limb

After the 3D model design and simulation stages, the SPA chambers were fabricated for the experimental analysis. The experiment was conducted using the SPA chamber unit to resemble the actual compression. For the validation of the SPA system model, the obtained simulated and experimental results were compared for a better understanding of the fabricated SPA chambers. A sensor-based SPA system was developed, consisting of SPA, a SPA controller, and monitoring software as shown in Figure 4. The exterior layer of the chambers was laminated with a woven-based textile shell with a dimension of 210 (width) × 460 (length) mm^2 to form the main part of the SPA unit. This was wrapped onto a mannequin leg for compression treatment simulation as depicted in Figure 4a. According to Li et al., the mannequin leg demonstrated similar contact pressure patterns to the human leg [34]. The force applied to the mannequin leg was measured to provide an accurate pressure reading. Force-sensitive resistor (FSR) was attached to the medial side of the lower leg, about 20 cm above the ankle, where the gastrocnemius muscle's tendinous and muscular parts separate as shown in Figure 4b. Next, the pressure exerted on the skin by the SPA system on the force sensor was assessed. A portable air compressor was attached to the pressure sensor and solenoid valve to operate the SPA system. Pressure sensors (model no. MPS20N0040D, Soldered Electronics, Osijek, Croatia) were used to monitor the supply pressure. The SPA controller comprised an air pump, Step-Down voltage regulator (LM2596 SIMPLE Switcher Power Converter 150-kHz, Digi-Key Electronics, Thief River Falls, MN, USA), pressure sensor, data acquisition control board (Arduino Pro Mini, Digi-Key Electronics, Thief River Falls, MN, USA), and solenoid valve. The hardware working model was built as shown in Figure 4c.

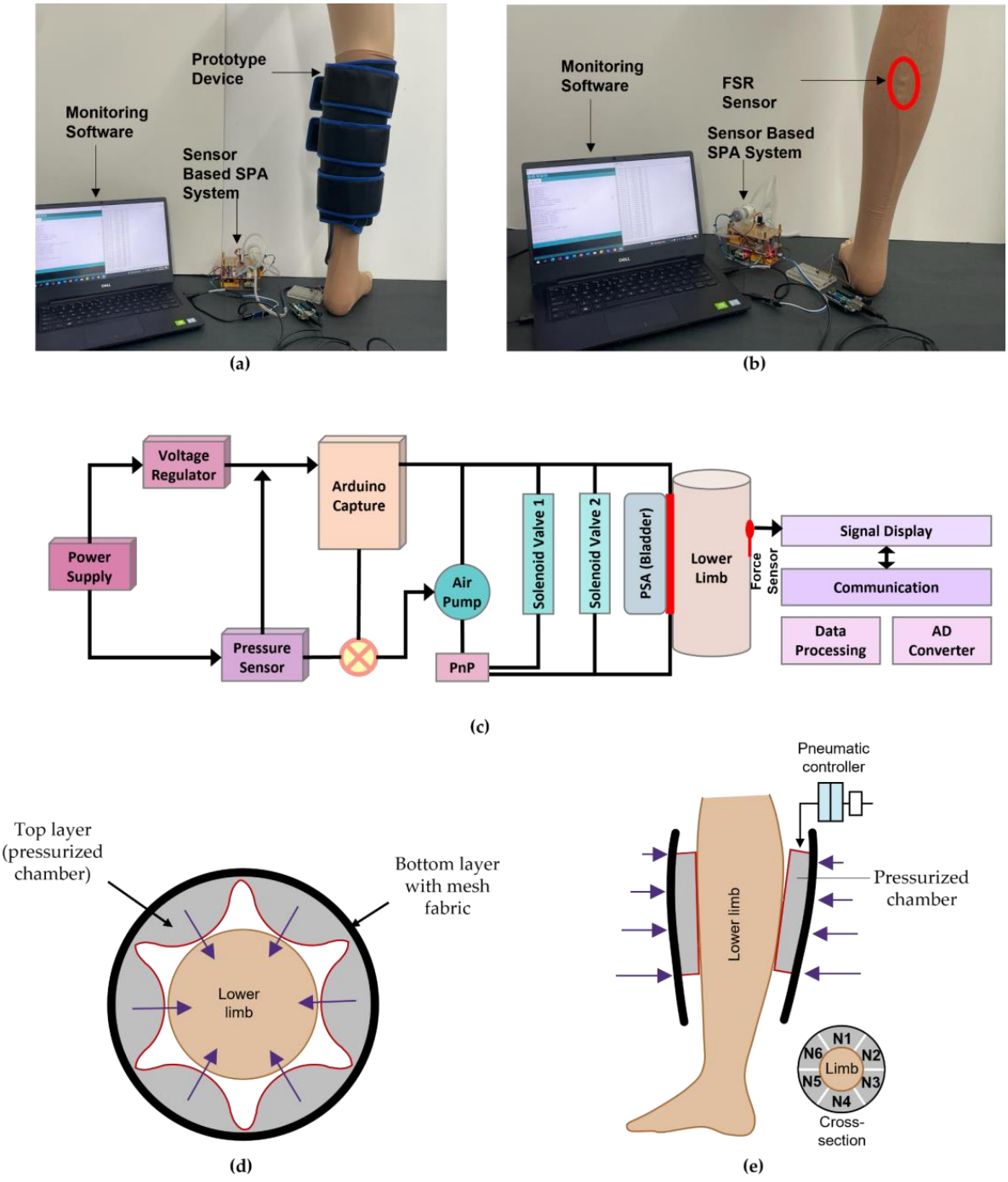


Figure 4. The experimental setup to evaluate pressure transmission: (**a**) monitoring system for mannequin leg with SPA chamber; (**b**) the FSR sensor embedded inside the skin layer at gastrocnemius muscle; (**c**) schematic diagram of SPA testing system, pressure transmission monitor; (**d**) schematic diagram of SPA with six airtight chambers; and (**e**) schematic diagram of lower-limb SPA system.

The experimental platform developed to calculate the 3D deformation profile of the chamber concerning their inflation height is shown in Figure 5. The test rig consists of a distance laser meter (Class 2635 nm, <1 mV, Accuracy $\pm$ 1 mm) that was fixed onto the retort stand vertically to secure its position. Since the greatest deformation for uniformly distributed pressure occurred at the center of the simulation result, the laser head was aimed at the chamber's center. The SPA chamber was placed horizontally on a flat table to measure the deformation. The laser point coincides with the center of the chamber.

The initial height, h_0 of the chamber was measured. The SPA chambers were inflated in increments of 1.0 mL air volume for 23 s inflation and 7 s holding and 7 s deflation. The deformed height, h_i, at every 1 s interval was recorded. This test was repeated for five complete cycles at the designated position, and the average values for deformation were included in the result.

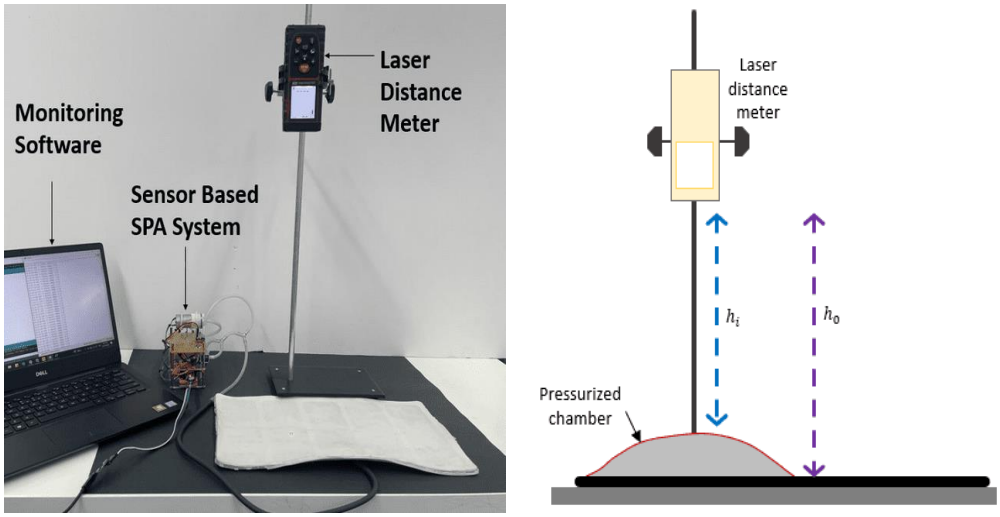


Figure 5. Experimental setup: (**a**) real-time arrangement and (**b**) schematic diagram for measuring the inflation height.

2.5. Data Analysis

To assess the reliability between simulated and experimental conditions, the intraclass correlation coefficient (ICC) was used. With this, 95% confidence intervals were calculated using Microsoft Excel based on an absolute agreement: specifically, a mixed-effect model (ICC 3,1). The classification of ICC defined the degree of consistency used to interpret ICC value: excellent (>0.9), good (0.76–0.9), moderate (0.5–0.75), and poor (lower than 0.50) [35].

Bland–Altman analysis with 95% limits of agreement (LoA) was performed to access the agreements between datasets obtained during the two conditions. The scatterplot was constructed with partiality and the LoA is shown in the plot for the parameters registered. The mean score is represented on the x-axis, and the difference between two measurements (mean of the differences) is plotted on the y-axis. The 95% LoA is defined as ± 1.96 standard deviation (SD) (BA2). The average difference (Diff), the standard deviation of the differences (SD), and lower and upper 95% confidence level (CI) were from the formula: upper 95% CI = Diff $-$ 1.96 $\times$ SD; lower 95% CI = Diff + 1.96 $\times$ SD [36]. The width of the boundaries of agreement and the distance of the mean through these differences were used to interpret measurement errors. An acceptable agreement between these two measurements was indicated when 95% of the data fell inside the LoA [37]. No significant difference between the measurements was reflected in case the line of equality was within the interval [38].

3. Results

3.1. Simulated 3D Deformation Results of the Proposed Chamber Using Three Different Materials

Pressure variation was employed to investigate the associated mechanisms of the SPA performance design parameter during the inflation–deflation cycle. The pressure variation can also be utilized to evaluate the developed prototype model. Figure 6 shows the simulation result of the SPA chamber's detected operating rhythms using the three silicone rubber materials. This result demonstrates the applicability of the developed 3D model in the prediction of the pneumatic pressure and its variation during the inflation–

deflation cycles of the SPA system for the three different materials. The variation profile was based on the pressure supply at the inner wall of the SPA chamber.

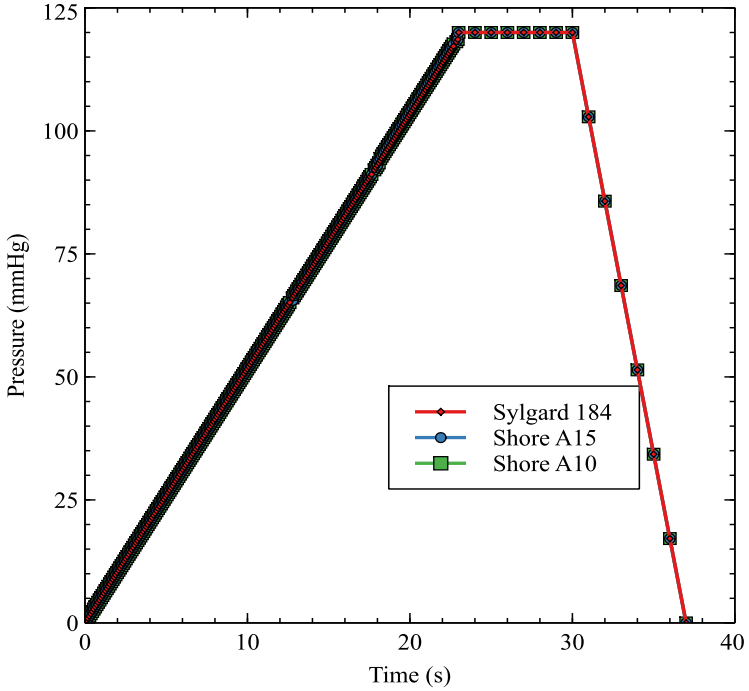


Figure 6. Detected pneumatic pressure during simulated inflation–holding–deflation cycle for three different materials by the SPA system.

The SPA was simulated from 0 to 120 mmHg. The deformation result of the SPA system during inflation–holding–deflation was obtained, and the simulation of the three different silicone-based materials was compared. The contour of deformation during inflation at 27 s of the three different materials is shown in Figure 7. Comparatively, the deformation in the y direction was considered. At the initial state, the deformation started at approximately 14 to 16 mm for each material. The deformation of each chamber is represented by the color map. A red indication represents high pressure and blue low pressure. The top part of the chamber revealed significant deformation compared to the bottom part. This finding is due to the different thickness inputs for the upper and lower part. The maximum pressure appears at the center of the chamber compared to the area near the surrounding edge.

The average deformation varied between 0 to 23 mm: A10 Shore silicone had the highest inflation with a maximum deformation of 25.34 mm, followed by A15 Shore with a maximum deformation at 24.68 mm, and Sylgard 184 with a maximum deformation of 21.38 mm. Figure 8 indicates that A10 Shore silicone could result in higher deformation under the same air pressure as compared to A15 Shore and Sylgard 184. The material with the higher deformation is used to produce the main part of the SPA. Xavier et al. [28], in an overview of the recent development of soft actuators, reported that low silicone hardness causes greater deformation at lower pressure values. This will reduce the time required to achieve the shape transition and provide the desired force toward the leg.

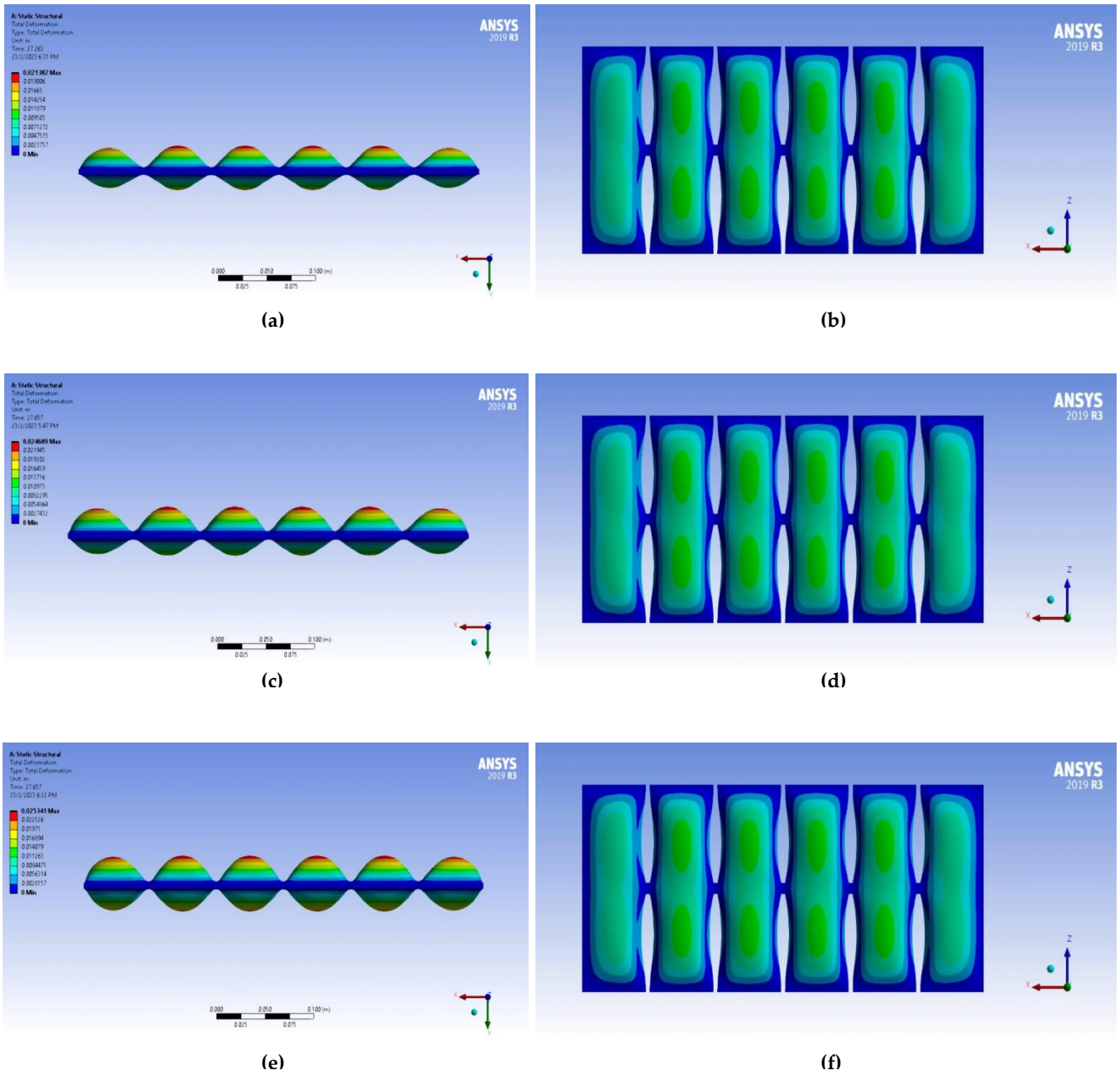


Figure 7. Deformation comparison of three different silicone rubber of the SPA chamber from the FEM simulation models. Slygard 184: (**a**) side view and (**b**) bottom view. Food-grade silicone (A15 Shore): (**c**) side view and (**d**) bottom view. Food-grade silicone (A10 Shore): (**e**) side view and (**f**) bottom view.

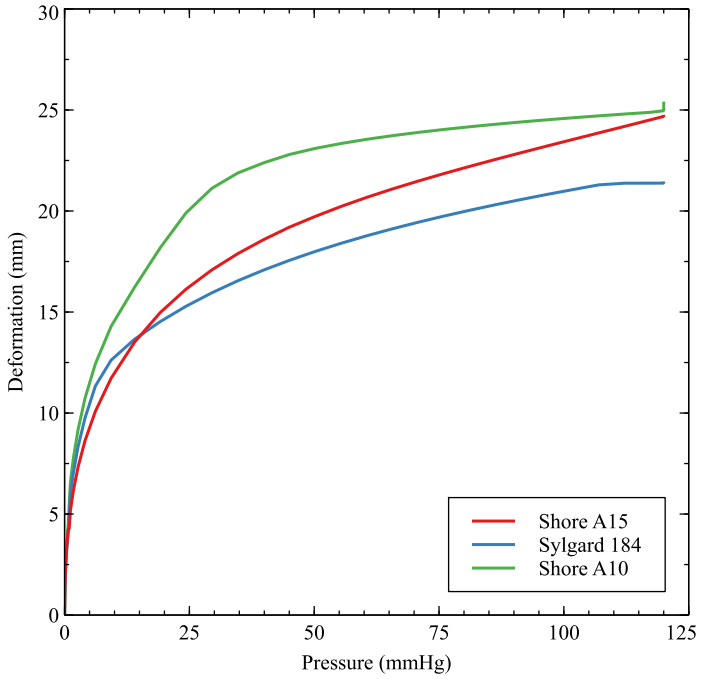


Figure 8. The behavior of three silicone elastomers from the simulation results: deformation vs. pressure.

3.2. Comparison and Validation of Simulation and Experimental Results

To compare and validate the simulation and experimental results, we performed an experiment on a mannequin leg. It was important to calculate the pressure transferred by the SPA chamber onto the leg and to evaluate the efficiency of the SPA chamber performance based on the selected material. This will depict the inflatable SPA chamber in contact with human skin in delivering the required pressure. Based on the simulation results, we fabricated the SPA chamber using food-grade silicone with a Shore hardness of A10 and A15. The material for the upper and bottom layers was A10 Shore food-grade silicone, and A15 Shore food-grade silicone, respectively. The experimental setup discussed in Section 2.4 was used to measure the pressure transmission of the SPA chamber. The interface pressure was expressed as a function of force exerted on the skin measured using an FSR sensor. The experimental result of the maximum deformation during the inflation of the SPA chamber was compared against the FEM results for maximum deformation in relation to the supplied pressure.

The reliability showed a good correlation for material deformation ICC > 0.9 for both conditions. There was no significant difference in the average deformation between the two testing methods ($p > 0.05$). For the Bland–Altman plot, the differences between the simulation and experimental for material parameters (i.e., deformation) are illustrated in Figure 9. The three lines represent the mean differences. The solid line represent bias and the two dash line are limit of agreements mean +1.96 SD (upper interval) and mean −1.96 SD (lower interval). The LoA for material deformation was (95% CI 2.83 to −1.33). From the graph, the scatterplot also demonstrates that most of the points were evenly distributed within the interval in material deformation. There is only one outlier detected beyond the interval. However, most of the deformation points were within LoA.

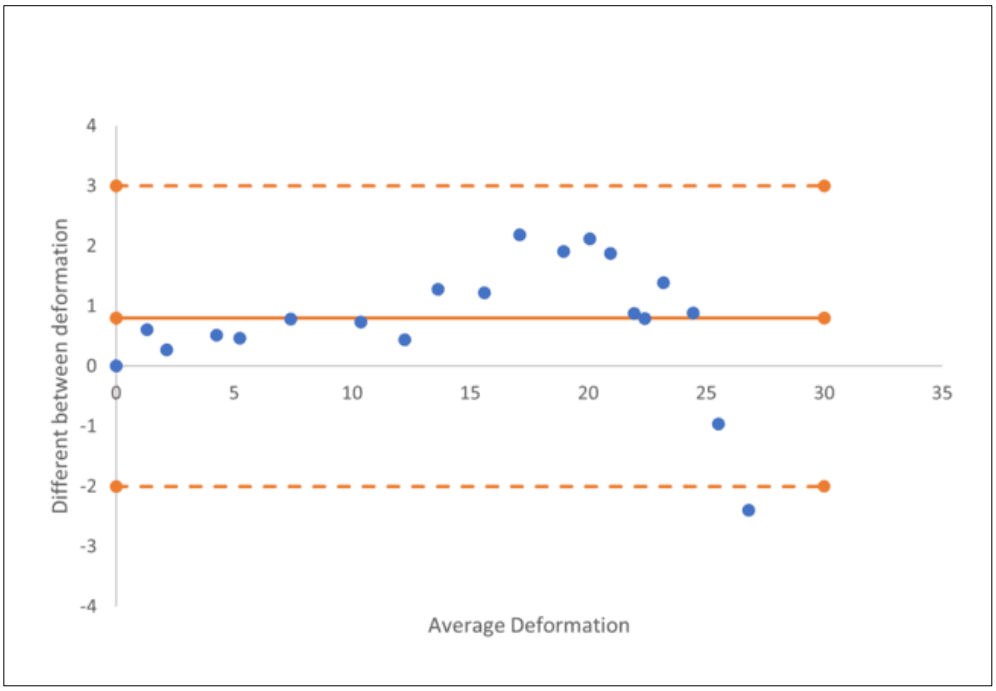


Figure 9. The Bland-Altman plot of the SPA unit deformation for simulation and experiment.

4. Discussion

The behavior of the SPA has been widely assessed using FEM analysis to optimize its design. The performance of SPA strongly depends on the design parameters and material used [26]. Considering that food-grade silicone has the same properties as commercial silicone, including the ability to provide effective pressure transfer as well as being non-hazardous, this study aimed to anticipate the influence of the material selection of three silicone elastomeric rubbers composed of commercial and food-grade silicone. The findings showed that A10 Shore silicone has the highest deformation compared to A15 Shore and Sylgard 184. These outcomes are in agreement with the properties of A10 Shore which has a lower Shore hardness than A15 Shore and Sylgard 184 [39]. Benjamin et al. [40] stated that very large deformation is exerted on the inflatable actuators and, to avoid high pressure, elastomers with a low Shore hardness are preferred.

Silicone is an isotropic material with unique mechanical properties, such as Young's modulus, Poisson's ratio, and shear modulus, which can lead to dissimilar deformation during inflation. A10 Shore has the lowest Young's modulus compared to A15 Shore and Sylgard 184. A10 Shore is softer than other elastomers, requiring lower pressure levels to achieve the desired deformation of the soft actuators. In a study on the characterization of pneumatic muscle actuators, Antonio et al. [41] discovered that materials with a low Young's modulus create greater deformation and force when stimulated. The amount of compressed gas that must be introduced into the chamber to reach the required pressure is specified by the elastomeric material's deformation [42].

This study analyzed the reliability between the simulated and experimental conditions using a relative measure. The mean difference between the two conditions in this study was illustrated and analyzed using a Bland–Altman approach. The Bland–Altman plotting was used to compare a new measurement instrument or procedure to an approved method. In a study by Jared et al. [43], the authors applied a Bland–Altman and correlation analysis to assess the two methods of blood pressure measurement. The mean difference between the two conditions in this study was illustrated and analyzed using a Bland–Altman plot method.

Based on the Bland–Altman plot, the deformation points in both the simulation and experimental were within the intervals and limits of agreement (LoA). The findings showed

an acceptable agreement when testing the method of deformation between the simulation and experimental conditions. There was no apparent proportional partiality, implying that the differences between the two methods of testing occurred at random over the pressure range. A study by Yang Song et al. [44] on the validation of a 3D finite element (FE) coupled model of the foot and sports shoe reported most of the points were scattered between ±1.96 SD to indicate the two approaches are in good agreement.

The high ICC values for the deformation parameters indicated that the SPA unit was dependable. No clear agreement has been reported on the applicable standard values for accepted reliability using ICC. A study by Fleiss considered ICC $\geq$ 0.75 as excellent, 0.75~0.40 as good to moderate, and <0.40 as poor [45].

Overall, the SPA chamber fabricated using food-grade silicone was able to apply interface pressure on the skin for a pressure range of 0–120 mmHg. The pressure range corresponds to the literature's interface pressure for compression therapy [46]. The outcomes showed that the model accurately captured the physical system in this pressure range. Although the results show that the SPA chamber can generate high skin interface pressure, determining the optimal pressure is still crucial in treating venous disease. Therefore, an appropriate approach to measure the interface pressure for a desired treatment should be proposed. However, this would rely on the stiffness of the skin; the modulus of the fat and muscle layers must be taken into consideration when determining how to inflate the SPA chamber in a clinical setting [47]. The results of the simulation study and experimental testing showed that the SPA system's silicone material stiffness had a significant impact on how the device deformed and how much pressure it applied to the skin.

The fabrication of soft actuators is continually evolving to further increase the prevalence of readily available soft robots among a wider group of professionals [48]. From this perspective, soft actuators need to be more affordable, safer, lighter, and more accessible. The proposed pneumatic soft actuator system was fabricated using readily available food-grade silicone. The system applicability is evaluated using FEM and experimental testing. Through this study, a few significant contributions were highlighted:

- This SPA model presented the soft, robust, biocompatible, and non-hazardous materials that have the elasticity properties of commercial silicone, and the extreme deformation change accompanying a pressure transition. The materials have high tensile strengths similar to conventional silicone-based elastomers—up to 1000%. These features have the potential to produce higher deformation with excellent tear resistance while maintaining the appropriate compression pressure on the calf.
- The proposed system is a simple and lightweight sensor-based SPA system with the dimensions of 10 cm in length, 8 cm in width, and 6 cm in height. This system offers the option of employing a simple, lightweight pump with adjustable cycle time and pressure supply settings for individual comfort. It is an appropriate compression device for offering safe and effective compression therapy while being lightweight enough for the user to carry. This prototype can serve as a new rehabilitation tool that can improve the quality of life for individuals with lower-limb disabilities. The use of these devices can potentially reduce the need for traditional physical therapy, leading to more efficient and cost-effective treatment options.
- We provide a comprehensive analysis by considering the inner wall pressure distribution in simulation and anticipate actual compression to the calf. With the comparison of the inner wall pressure and the pressure transferred by the SPA chamber onto a mannequin leg, we can determine the compression capability before clinical testing. The maximum deformation of the 3D model at the inner wall of the chamber was 25.34 mm, whereas the maximum experimental deformation of the SPA chamber was 28 mm. It can be seen from the results that the experimental results for the SPA system show a more than 0.9 reliability agreement with the simulation data for the range of pressure 0–120 mmHg.
- The research has the potential to contribute to improvements in health and socioeconomic development. The use of soft pneumatic actuators can lead to better rehabilita-

tion outcomes, which can improve the quality of life for individuals with lower-limb disabilities. Improved rehabilitation outcomes can also lead to increased productivity and reduced healthcare costs. The use of cost-effective and efficient treatment options can potentially benefit low- and middle-income countries, where access to traditional physical therapy may be limited.

5. Conclusions

In this study, an SPA system was designed and developed to detect and visualize the interface pressure induced by the SPA chamber. FEM was used in choosing the design parameters and silicone rubber materials that are appropriate for SPA applications with a minimum of 1N force. The modeling of soft actuators using A10 Shore food-grade silicon demonstrates the material's potential as a major component for soft actuators. A10 Shore silicone produces higher deformation up to 28 mm during inflation. The simulation model was compared with the SPA system and the deformation behavior was observed. The reliability showed a good correlation for material deformation, with ICC > 0.9 for both conditions. The simulation and experimental results show an excellent agreement of pressure transmission on the skin for the pressure range of 0–120 mmHg. The developed model is useful for the FEM simulation-based design optimization of soft actuators, by investigating the relationship between pressure and deformation. Therefore, it is proposed that food-grade silicone is an acceptable alternative for the fabrication of SPA as it can apply interface pressure on the skin.

6. Limitation and Future Work

The present study had some limitations. This 3D model simulation did not include the fluid–structure interaction (FSI) between the fluid and the solid, where the pressure flow behavior inside the SPA would be analyzed. Future studies should include the simulation of the pressure from the SPA inlet using an FSI analysis to determine the appropriate pressure to be applied on the skin surface. Moreover, the experimental testing was performed using a single mannequin leg. It is suggested that future studies should consider studying the pressure transmission on the human leg profile with different types of skin stiffness and fat layers. One limitation of conducting experiments on the stress–pressure relationships of soft pneumatic actuators is the difficulty in accurately measuring the internal pressure within the actuator. Initially, the experimental pressure was indirectly obtained through the FSR sensor. Direct uniaxial tension should be quantified using a tensometer to attain the stress–strain curve of the SPA. Lastly, the pain and comfort assessment as well as experimental testing of the established SPA model on human subjects can be conducted to further test its deformation capabilities.

Author Contributions: Conceptualization, H.B., K.H., N.A.A.R., R.M.R., A.A.K., M.'A.A., A.T. and D.R.; Methodology, H.B., K.H., A.A.K. and M.'A.A.; Software, H.B., A.A.K. and D.R.; Validation, H.B., K.H., N.A.A.R., R.M.R. and M.'A.A.; Formal analysis, H.B. and A.A.K.; Investigation, H.B., A.A.K. and M.'A.A.; Resources, H.B., K.H., N.A.A.R., R.M.R., A.T. and D.R.; Data curation, H.B.; Writing—original draft, H.B. and K.H.; Writing—review & editing, H.B., K.H., N.A.A.R. and R.M.R.; Visualization, H.B. and K.H.; Supervision, H.B., K.H., N.A.A.R., R.M.R. and D.R.; Project administration, K.H., N.A.A.R., R.M.R. and A.T.; Funding acquisition, A.T. All authors have read and agreed to the published version of the manuscript.

Funding: This research was funded by Medical Revolution Sdn Bhd, Kuala Lumpur, Malaysia.

Institutional Review Board Statement: Not applicable.

Informed Consent Statement: Not applicable.

Data Availability Statement: https://drive.google.com/drive/folders/1HKmxOBrZCcjLmJaGD8SsZHEO9P1y5_Nv?usp=share_link, accessed on 20 February 2023.

Conflicts of Interest: The authors declare no conflict of interest.

References

1. McGuine, T.A.; Post, E.G.; Hetzel, S.J.; Brooks, M.A.; Trigsted, S.; Bell, D.R. A Prospective Study on the Effect of Sport Specialization on Lower Extremity Injury Rates in High School Athletes. *Am. J. Sports Med.* **2017**, *45*, 2706–2712. [CrossRef] [PubMed]
2. Bramah, C.; Preece, S.J.; Gill, N.; Herrington, L. Is There a Pathological Gait Associated with Common Soft Tissue Running Injuries? *Am. J. Sports Med.* **2018**, *46*, 3023–3031. [CrossRef] [PubMed]
3. Bisciotti, G.N.; Volpi, P.; Amato, M.; Alberti, G.; Allegra, F.; Aprato, A.; Artina, M.; Auci, A.; Bait, C.; Bastieri, G.M.; et al. Italian Consensus Conference on Guidelines for Conservative Treatment on Lower Limb Muscle Injuries in Athlete. *BMJ Open Sport Exerc. Med.* **2018**, *4*, e000323. [CrossRef] [PubMed]
4. Ishøi, L.; Krommes, K.; Husted, R.S.; Juhl, C.B.; Thorborg, K. Diagnosis, Prevention and Treatment of Common Lower Extremity Muscle Injuries in Sport—Grading the Evidence: A Statement Paper Commissioned by the Danish Society of Sports Physical Therapy (DSSF). *Br. J. Sports Med.* **2020**, *54*, 528–539. [CrossRef] [PubMed]
5. Schwellnus, M.P.; Swanevelder, S.; Jordaan, E.; Derman, W.; Van Rensburg, D.C.J. Underlying Chronic Disease, Medication Use, History of Running Injuries and Being a More Experienced Runner Are Independent Factors Associated with Exercise-Associated Muscle Cramping: A Cross-Sectional Study in 15,778 Distance Runners. *Clin. J. Sport Med.* **2018**, *28*, 289–298. [CrossRef] [PubMed]
6. Ostrowski, J.; Purchio, A.; Beck, M.; Leisinger, J. Effectiveness of Salted Ice Bag Versus Cryo-Compression on Decreasing Intramuscular and Skin Temperature Authors. *J. Sport Rehabil.* **2017**, *28*, 588–595. [CrossRef]
7. Hilberg, T.; Ransmann, P.; Hagedorn, T. Sport und Venöse Thromboembolie. *Dtsch. Arztebl. Int.* **2021**, *118*, 181–187. [CrossRef]
8. Youn, Y.J.; Lee, J. Chronic Venous Insufficiency and Varicose Veins of the Lower Extremities. *Korean J. Intern. Med.* **2019**, *34*, 269–283. [CrossRef]
9. Berszakiewicz, A.; Sieroń, A.; Krasiński, Z.; Cholewka, A.; Stanek, A. Compression Therapy in Venous Diseases: Current Forms of Compression Materials and Techniques. *Postep. Dermatol. Alergol.* **2021**, *37*, 836–841. [CrossRef]
10. Rosalia, L.; Lamberti, K.K.; Landry, M.K.; Leclerc, C.M.; Shuler, F.D.; Hanumara, N.C.; Roche, E.T. A soft robotic sleeve for compression therapy of the lower limb. In Proceedings of the 2021 43rd Annual International Conference of the IEEE Engineering in Medicine & Biology Society (EMBC), Guadalajara, Mexico, 1–5 November 2021; pp. 2258–2265.
11. Chua, M.C.H.; Lim, J.H.; Yeow, R.C.H. Design and Characterization of a Soft Robotic Therapeutic Glove for Rheumatoid Arthritis. *Assist. Technol.* **2019**, *31*, 44–52. [CrossRef]
12. Thalman, C.M.; Lee, H. Design and Validation of a Soft Robotic Ankle-Foot Orthosis (SR-AFO) Exosuit for Inversion and Eversion Ankle Support. In Proceedings of the 2020 IEEE International Conference on Robotics and Automation (ICRA), Paris, France, 31 May–31 August 2020; pp. 1735–1741. [CrossRef]
13. Zhu, M.; Do, T.N.; Hawkes, E.; Visell, Y. Fluidic Fabric Muscle Sheets for Wearable and Soft Robotics. *Soft Robot.* **2020**, *7*, 179–197. [CrossRef] [PubMed]
14. Xiao, C.; Jahanian, O.; Schnorenberg, A.; Slavens, B.; Hsiao-Wecksler, E. Design and Biomechanical Evaluation Methodology of Pneumatic Ergonomic Crutch. In Proceedings of the 2017 Design of Medical Devices Conference, Minneapolis, MN, USA, 10–13 April 2017; pp. 10–11. [CrossRef]
15. Zhao, S.; Liu, R.; Fei, C.; Guan, D. Dynamic Interface Pressure Monitoring System for the Morphological Pressure Mapping of Intermittent Pneumatic Compression Therapy. *Sensors* **2019**, *19*, 2881. [CrossRef] [PubMed]
16. Zhao, S.; Liu, R.; Wu, X.; Ye, C.; Zia, A.W. A Programmable and Self-Adaptive Dynamic Pressure Delivery and Feedback System for Efficient Intermittent Pneumatic Compression Therapy. *Sens. Actuators A Phys.* **2020**, *315*, 112285. [CrossRef]
17. Miriyev, A.; Stack, K.; Lipson, H. Soft Material for Soft Actuators. *Nat. Commun.* **2017**, *8*, 596. [CrossRef]
18. Craddock, M.; Augustine, E.; Konerman, S.; Shin, M. Biorobotics: An Overview of Recent Innovations in Artificial Muscles. *Actuators* **2022**, *11*, 168. [CrossRef]
19. Coyle, S.; Majidi, C.; Leduc, P.; Hsia, K.J. Bio-Inspired Soft Robotics: Material Selection, Actuation, and Design. *Extrem. Mech. Lett.* **2018**, *22*, 51–59. [CrossRef]
20. Pagoli, A.; Chapelle, F.; Antonio, J.; Ramon, C.; Lapusta, Y.; Pagoli, A.; Chapelle, F.; Antonio, J.; Ramon, C.; Mezouar, Y.; et al. Review of Soft Fluidic Actuators: Classification and Materials Modeling Analysis. *Smart Mater. Struct.* **2022**, *31*, 013001. [CrossRef]
21. Huri, D.; Mankovits, T. Comparison of the Material Models in Rubber Finite Element Analysis. *IOP Conf. Ser. Mater. Sci. Eng.* **2018**, *393*, 012018. [CrossRef]
22. Mourtzis, D. Simulation in the Design and Operation of Manufacturing Systems: State of the Art and New Trends. *Int. J. Prod. Res.* **2020**, *58*, 1927–1949. [CrossRef]
23. Fang, J.; Yuan, J.; Wang, M.; Xiao, L.; Yang, J.; Lin, Z.; Xu, P.; Hou, L. Novel Accordion-Inspired Foldable Pneumatic Actuators for Knee Assistive Devices. *Soft Robot.* **2020**, *7*, 95–108. [CrossRef]
24. Li, H.; Cheng, L. Preliminary Study on the Design and Control of a Pneumatically-Actuated Hand Rehabilitation Device. In Proceedings of the 2017 32nd Youth Academic Annual Conference of Chinese Association of Automation (YAC), Hefei, China, 19–21 May 2017; pp. 860–865. [CrossRef]
25. Soft Robotics Toolkit Soft Robotics Toolkit. Available online: https://softroboticstoolkit.com/ (accessed on 20 November 2022).
26. Maruthavanan, D.; Seibel, A.; Schlattmann, J. Fluid-Structure Interaction Modelling of a Soft Pneumatic Actuator. *Actuators* **2021**, *10*, 163. [CrossRef]
27. Steck, D.; Qu, J.; Kordmahale, S.B.; Tscharnuter, D.; Muliana, A.; Kameoka, J. Mechanical Responses of Ecoflex Silicone Rubber: Compressible and Incompressible Behaviors. *J. Appl. Polym. Sci.* **2019**, *136*, 1–11. [CrossRef]

28. Xavier, M.S.; Fleming, A.J.; Yong, Y.K. Finite Element Modeling of Soft Fluidic Actuators: Overview and Recent Developments. *Adv. Intell. Syst.* **2021**, *3*, 2000187. [CrossRef]
29. Pini, L. *Geometry Optimization for Biaxial Testing of Polydimethylsiloxane SYLGARD 184 and Finite Element Modelling*; Politecnico di Milano: Milan, Italy, 2020.
30. Product, A. Axel Products Physical Testing Services. Available online: http://www.axelproducts.com/ (accessed on 20 November 2022).
31. Di Lecce, M.; Onaizah, O.; Lloyd, P.; Chandler, J.H.; Valdastri, P. Evolutionary Inverse Material Identification: Bespoke Characterization of Soft Materials Using a Metaheuristic Algorithm. *Front. Robot. AI* **2022**, *8*, 790571. [CrossRef]
32. Guan, D.; Liu, R.; Fei, C.; Zhao, S.; Jing, L. Fluid-Structure Coupling Model and Experimental Validation of Interaction between Pneumatic Soft Actuator and Lower Limb. *Soft Robot.* **2020**, *7*, 627–638. [CrossRef] [PubMed]
33. Tawk, C.; Alici, G. Finite Element Modeling in the Design Process of 3D Printed Pneumatic Soft Actuators and Sensors. *Robotics* **2020**, *9*, 52. [CrossRef]
34. Li, Q.; Sun, G.; Chen, Y.; Chen, X.; Shen, Y.; Xie, H.; Li, Y. Fabricated Leg Mannequin for the Pressure Measurement of Compression Stockings. *Text. Res. J.* **2022**, *92*, 3500–3510. [CrossRef]
35. Fernández-González, P.; Koutsou, A.; Cuesta-Gómez, A.; Carratalá-Tejada, M.; Miangolarra-Page, J.C.; Molina-Rueda, F. Reliability of Kinovea® Software and Agreement with a Three-Dimensional Motion System for Gait Analysis in Healthy Subjects. *Sensors* **2020**, *20*, 3154. [CrossRef]
36. Liu, J.; Liu, Y.; Wang, J.; Zuo, X.; Wang, X.; Zhang, Y.; He, H. Dental Measurements Based on a Three-Dimensional Digital Technique: A Comparative Study on Reliability and Validity. *Arch. Oral Biol.* **2021**, *124*, 105059. [CrossRef] [PubMed]
37. Gerke, O. Reporting Standards for a Bland-Altman Agreement Analysis: A Review of Methodological Reviews. *Diagnostics* **2020**, *10*, 334. [CrossRef]
38. Lau, E. Accuracy of Bromocresol Green (BCG) Method for Plasma Albumin. Bachelor's Thesis, Norwegian University of Science and Technology, Trondheim, Norway, 2020.
39. Smooth-On Durometer Shore Hardness Scale. Available online: https://www.smooth-on.com/page/durometer-shore-hardness-scale/ (accessed on 20 November 2022).
40. Gorissen, B.; Reynaerts, D.; Konishi, S.; Yoshida, K.; Kim, J.W.; De Volder, M. Elastic Inflatable Actuators for Soft Robotic Applications. *Adv. Mater.* **2017**, *29*, 1604977. [CrossRef] [PubMed]
41. Carvalho, A.D.D.R.; Karanth, P.N.; Desai, V. Characterization of Pneumatic Muscle Actuators and Their Implementation on an Elbow Exoskeleton with a Novel Hinge Design. *Sens. Actuators Rep.* **2022**, *4*, 100109. [CrossRef]
42. Mosadegh, B.; Polygerinos, P.; Keplinger, C.; Wennstedt, S.; Shepherd, R.F.; Gupta, U.; Shim, J.; Bertoldi, K.; Walsh, C.J.; Whitesides, G.M. Pneumatic Networks for Soft Robotics That Actuate Rapidly. *Adv. Funct. Mater.* **2014**, *24*, 2163–2170. [CrossRef]
43. Leitner, J.; Chiang, P.H.; Dey, S. Personalized Blood Pressure Estimation Using Photoplethysmography: A Transfer Learning Approach. *IEEE J. Biomed. Health Inform.* **2022**, *26*, 218–228. [CrossRef] [PubMed]
44. Song, Y.; Cen, X.; Zhang, Y.; Bíró, I.; Ji, Y.; Gu, Y. Development and Validation of a Subject-Specific Coupled Model for Foot and Sports Shoe Complex: A Pilot Computational Study. *Bioengineering* **2022**, *9*, 553. [CrossRef] [PubMed]
45. Fleiss, J.L. *The Design and Analysis of Clinical Experiments*; John Wiley & Sons, Inc.: Hoboken, NJ, USA, 2014; Volume 43, pp. 43–44.
46. Zaleska, M.; Olszewski, W.L.; Jain, P.; Gogia, S.; Rekha, A.; Mishra, S.; Durlik, M. Pressures and Timing of Intermittent Pneumatic Compression Devices for Efficient Tissue Fluid and Lymph Flow in Limbs with Lymphedema. *Lymphat. Res. Biol.* **2013**, *11*, 227–232. [CrossRef]
47. Nandasiri, G.K.; Ianakiev, A.; Dias, T. Hyperelastic Properties of Platinum Cured Silicones and Its Applications in Active Compression. *Polymers* **2020**, *12*, 148. [CrossRef] [PubMed]
48. Walker, J.; Zidek, T.; Harbel, C.; Yoon, S.; Strickland, F.S.; Kumar, S.; Shin, M. Soft Robotics: A Review of Recent Developments of Pneumatic Soft Actuators. *Actuators* **2020**, *9*, 3. [CrossRef]

Disclaimer/Publisher's Note: The statements, opinions and data contained in all publications are solely those of the individual author(s) and contributor(s) and not of MDPI and/or the editor(s). MDPI and/or the editor(s) disclaim responsibility for any injury to people or property resulting from any ideas, methods, instructions or products referred to in the content.